






A Comparative Study of Conventional and Tripolar EEG for High-Performance Reach-to-Grasp BCI Systems

Ali Rabiee * ¹, Sima Ghafoori * ¹, Anna Cetera ¹, Walter Besio ¹, and Reza Abiri ¹

¹Dept. of Electrical, Computer and Biomedical Engineering, URI, Kingston, USA

Abstract

Objective. This study aims to enhance brain-computer interface (BCI) applications for individuals with motor impairments by comprehensively comparing the effectiveness of noninvasive tripolar EEG (tEEG) with conventional EEG technology. The focus is on accurately interpreting and decoding various grasping movements, such as power grasp and precision grasp. The goal is to determine which EEG technology is more effective in processing and translating grasp-related neural signals. *Approach.* The approach involved conducting an experiment on ten healthy participants who performed two distinct reach-and-grasp movements: power grasp and precision grasp, with a 'no-movement' condition serving as the baseline. Our research presents a thorough comparison between EEG and tEEG in decoding grasping movements. This comparison spans several key parameters, including signal-to-noise ratio (SNR), spatial resolution via functional connectivity, event-related potentials (ERPs), and wavelet time-frequency analysis. Additionally, our study involved extracting and analyzing statistical features from the wavelet coefficients, and both binary and multiclass classification methods were employed. Four machine learning algorithms—Random Forest (RF), Support Vector Machine (SVM), Extreme Gradient Boosting (XGBoost), and Linear Discriminant Analysis (LDA)—were used to evaluate the decoding accuracies. *Main results.* Our results indicated that tEEG demonstrated superior performance over conventional EEG in various aspects. This included a higher signal-to-noise ratio, enhanced spatial resolution, and more informative data in ERPs and wavelet time-frequency analysis. The use of tEEG led to notable improvements in decoding accuracy for differentiating movement types. Specifically, tEEG achieved around 90% accuracy in binary and 75.97% for multiclass classification. These results are markedly better than those from standard EEG, which recorded a maximum of 77.85% and 61.27% in similar tasks, respectively. These findings highlight the superior effectiveness of tEEG over conventional EEG in decoding grasp types and its competitive or superior performance in complex classifications compared with existing research.

Keywords: brain-computer-interface, motor impairments, tripolar EEG (tEEG), conventional EEG, grasping movements, machine learning

*These authors contributed equally to this work.

1 Introduction



Figure 1: (Left) tEEG electrode. (Right) Conventional EEG electrode.

Brain-computer interfaces (BCIs) represent a transformative technology, creating a direct communication link between neural activity and computer systems [1–3]. They offer substantial benefits to individuals with severe motor impairments, especially those resulting from spinal cord injuries, enhancing their quality of life through control over assistive devices and technologies. A key and challenging aspect in BCI applications is decoding human grasping intentions. This isn’t just about motor function; it integrates sensory perceptions, motor planning, and cognitive intentions [4]. The significance of accurately decoding these intentions extends beyond scientific interest, holding the potential to revolutionize assistive technologies and facilitate natural interactions for BCI users.

The act of reaching and grasping is central to human motor functions and crucial for daily tasks. This involves various brain areas: the parietal regions, including the anterior intraparietal sulcus, the premotor regions like the ventral premotor cortex, and the primary motor cortex [5, 6]. While grasping plays a pivotal role in our interactions, decoding its underlying complex neuronal mechanisms remains a primary objective in neuroscience [7]. Achieving this can transform numerous domains: from enhancing rehabilitation medicine [8–11] and advancing assistive technology [12–14] to designing intuitive brain-machine interfaces [15–17]. Grasping requires precise muscle and joint coordination, adapting to the object’s properties. Unraveling such intricate actions from brain signals is a challenging task. Many studies have explored the brain patterns linked to grasping actions in non-human primates [18–20] and humans using different acquisition modalities including invasive, such as electrocorticography (ECoG) [21] and noninvasive, such as functional magnetic resonance imaging (fMRI) [22, 23]. Additionally, numerous studies have demonstrated that noninvasive Electroencephalogram (EEG) signals can effectively decode reach-and-grasp actions. In this context, machine learning algorithms are pivotal in decoding complex neural data. Deep learning models like Convolutional Neural Networks (CNNs) and Recurrent Neural Networks (RNNs) offer advanced analysis capabilities but usually require large datasets, which can be challenging to collect from human participants [24]. Therefore, many studies prefer traditional models such as SVMs, Decision Trees, and LDA. These traditional algorithms are more manageable with smaller datasets and still significantly improve the accuracy of movement decoding and prediction [25]. Iturrate et al [26] utilized EEG to distinguish brain activation patterns during self-paced grasping tasks involving both precision and power grips, achieving 70% accurate single-trial decoding by using shrinkage LDA

(sLDA). Schwarz et al. [27] demonstrated that it’s possible to distinguish between three types of reach-and-grasp actions—palmar, pincer, and lateral grasp—using EEG neural correlates. The study achieved classification accuracies of up to 72.4% between grasp types and 93.5% for grasps versus no-movement conditions, supporting the potential use of this technique for more intuitive control of neuroprostheses. In another study by Xu et al [28], five distinct reach-and-grasp movements were decoded using movement-related cortical potentials (MRCPs) from noninvasive EEG signals. The movements included palmar, pinch, push, twist, and plug grasp. The study achieved a peak average accuracy of about 75% for grasping vs. no-movement conditions.

Despite the numerous studies utilizing EEG for decoding grasping movements, EEG often suffers from a low spatial resolution, complicating the precise localization of the source of neural activity due to the blurring effects primarily from different conductivities of the volume conductor [29]. It is also vulnerable to physiological disturbances caused by muscle contractions, eye movements, and heart activity, as well as technical artifacts like power-line noises or fluctuations in electrode impedances. These limitations directly impacts the decoding accuracy of motor intentions. Such a limitation emphasizes the need to explore advanced methods aimed at improving the spatial resolution of EEG data and increasing the signal-to-noise ratio. A promising solution is the use of tEEG, a novel technique involving an additional local reference electrode. The tripolar concentric ring electrode (TCRE) is roughly the same size as a conventional electrode. However, it consists of a central conductive disc with two electrically isolated rings surrounding it. The output signal from the TCRE is derived from a weighted sum of the outer ring subtracted from the central disc, which is then subtracted from sixteen times the difference between the inner ring and the central disc [30]. Compared to conventional disc electrode EEG, TCRE offers superior performance, with roughly 2.5 times higher spatial selectivity, 3.7 times higher signal-to-noise ratio, and approximately 12 times lower mutual information [31, 32]. There are other studies that demonstrated tEEG could effectively locate high-frequency activity in epilepsy patients, predominantly in the seizure onset zone, suggesting its potential utility in identifying epileptic brain regions [33, 34]. Also in [35], authors illustrated that tEEG significantly outperformed conventional disc electrodes in distinguishing individual finger movements, based on movement-related potentials (MRPs). Despite the potential benefits of tEEG, the use of tEEG in the realm of BCIs, particularly for decoding human grasping actions, remains largely unexplored, underlining the novelty and potential value of our study.

In this study, we embark on two pivotal explorations. Firstly, we conduct an in-depth comparison between conventional EEG and tEEG, examining parameters such as SNR, functional connectivity, and ERPs. Our visual illustrations, using topographical maps, aim to underscore the heightened spatial resolution of tEEG with respect to conventional EEG. As a subsequent step, we leverage the precision of wavelets to extract crucial features from the captured brain data. With the assistance of machine learning models, our overall goal is to enhance the decoding accuracy of grasping intentions. Through these endeavors, our research strives to emphasize the superiority of tEEG as a novel non-invasive neuroimaging technique in capturing brain signals and their mutual connectivities as well as the innovative potential of using wavelets technique in interpreting them.

2 Materials and Methods

A total of ten healthy volunteers, aged between 22 and 35 years consisting of five males and five females, participated in this study. The study was non-invasive and received approval from the Institutional Review Board (IRB). All participants had no known prior medical conditions and possessed normal or corrected-to-normal vision. They were thoroughly briefed about the study’s objectives. Before initiating any recordings, each participant provided informed consent, ensuring they understood the research’s purpose and procedures. The tasks they undertook involved performing grasping movements, specifically targeting objects such as a bottle or pen.

2.1 Experimental Setup and Paradigm

To thoroughly study the neural activity associated with natural vision-driven grasping tasks, we established a novel and comprehensive experimental setup and study protocol. Our experimental setup consists of a 3D-engineered, motorized turntable divided into three segments for displaying two objects (a bottle and a pen) as well as an empty space for a no-object scenario. A notable advancement in our system compared to other studies is the incorporation of innovative smart eyeglasses equipped with a special film that alternates between clear and opaque. This feature crucially reduces any potential anticipatory bias. Participants were comfortably seated, hands facing down, and placed 30 cm from the object’s center (Figure 1a). As illustrated in Figure 1c, following a three-second observation period accompanied by a buzzing sound signal, the participants commenced the grasping phase. The turntable then rotated to the next object or no-object condition randomly, during which the eyeglasses turned opaque, thus preparing for the subsequent phase.

2.2 Data Acquisition

EEG data acquisition was realized using the Unicorn Hybrid Black Bluetooth amplifier, capturing data at a rate of 250 samples per second per channel. Prior to initiating each session, skin-to-electrode impedance was assured to be below $10k\Omega$ to optimize data integrity. While Alzahrani’s work [35] demonstrated that only a single TCRE electrode at the C3 motor area location was sufficient for classifying imaginary finger movements, our study extends this approach by also considering additional brain regions such as parietal, central, and frontal areas, which play distinct and vital roles in the various stages of grasping tasks, from planning to execution [36]. To this end, we have strategically placed four TCREs at the P3, C3, C4, and F5 locations based on the 10-20 system, concurrently capturing tEEG and conventional EEG data [37]. Reference and ground electrodes were fixed at the left and right mastoids, respectively. Each participant underwent 50 trials for each condition, allowing us to gather a detailed and extensive dataset for further analysis.

2.3 Preprocessing

Data analysis was diligently executed utilizing custom Python scripts, leveraging functions from the ‘mne’ package [38]. Initially, the data underwent a high-pass filter at 1Hz to minimize signal drifts [39]. Following this foundational step, the recordings were bandpass filtered using a Finite Impulse

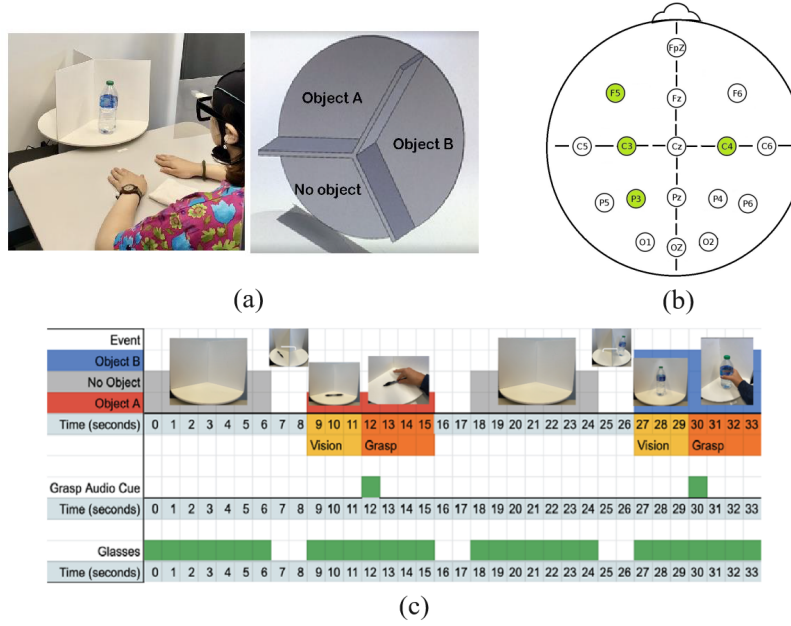


Figure 2: Experimental setup and paradigm for reach-and-grasp tasks. (a) Platform components, (b) an illustration of a 16-channel EEG sensor layout with the 4 electrodes (in green) which are used in the study to decode grasp movements, and (c) The experimental paradigm based on the audio cue. Objects A and B are randomly selected from a bottle and pen that requires power and precision grasps respectively.

Response (FIR) filter of order 20, spanning a frequency range of 1Hz—60Hz [40, 41]. This was paired with a notch filter targeting the elimination of the omnipresent 60Hz line noise.

Post the spectral filtering, wavelet denoising, an advanced signal processing technique, was implemented to further refine the quality of the EEG recordings. As shown by the authors in [42], wavelet denoising can be beneficial in EEG signals by removing noise while preserving salient features associated with underlying neuronal activities. For our denoising procedure, we utilized the Daubechies wavelet, specifically the 'db8' waveform, known for its excellent localization properties in both the time and frequency domains [43]. The 'db8' wavelet has been identified as the most effective wavelet for noise reduction in EEG signals when analyzing data from healthy subjects [44]. This particular wavelet is distinguished by its superior ability to eliminate extraneous noise, enhancing the clarity and reliability of EEG readings[45].

With the denoised signals in place, the subtraction of the mean reference and a detrending process was performed, aiming to counteract the introduction of spurious trends in the spectral data [46]. To ensure a consistent scale across data, the signals were subjected to Z-score normalization. This technique is essential for ensuring that EEG data is uniform across different measurements, which significantly contributes to improving the accuracy and effectiveness of both traditional machine learning and advanced deep learning models [47].

For a focused examination of movement-related activity, the data were meticulously segmented to capture the temporal window spanning 1 second before to 1 second after movement onset. Cul-

minating the preprocessing pipeline, an Independent Component Analysis (ICA) was administered [48, 49]. This sophisticated technique identified and eliminated components tainted by physiological or non-physiological noise extraneous to EEG signals, ensuring the highest fidelity in data quality for subsequent analytical endeavors.

2.4 Comparative Analysis

The foundational aspect of this study revolves around a comprehensive comparison between conventional EEG and tEEG technologies. Before delving into classification-based analyses, it is crucial to discern the inherent differences and potential advantages one technology may offer over the other. This section presents the methodologies employed to undertake such comparative analyses, focusing on four pivotal metrics: SNR, functional connectivity, time domain analysis using Event-Related Potentials (ERP), and Time-Frequency analysis using wavelets.

2.4.1 Signal-to-Noise Ratio (SNR)

In evaluating the efficacy of our preprocessing steps, we analyzed the SNR for both EEG and tEEG configurations across multiple channels. This analysis aimed to verify if the tEEG setup indeed offers enhanced signal quality compared to the standard EEG. For calculating SNR, we compared the wavelet-denoised signal to the noise, which is determined as the difference between the original signal and its denoised version. The SNR is computed using the formula:

$$\text{SNR} = 20 \times \log_{10} \left(\frac{\text{RMS of the Signal}}{\text{RMS of the Noise}} \right)$$

Here, RMS represents the Root Mean Square. In the context of a continuous waveform, the RMS is the square root of the mean power of the signal. For a discrete sequence, it refers to the square root of the sum of the squares over the total data points. Both EEG and tEEG data underwent SNR computation across all channels. It’s noteworthy to mention that the presented results represent grand averages accumulated from all subjects, ensuring a comprehensive overview. The data used for this analysis was specifically segmented around the peri-movement time frame.

2.4.2 Frequency-Domain Functional Connectivity Analysis using Coherence

Functional connectivity among channels was assessed using the coherence method, which quantifies the degree of synchrony between pairs of signals in the frequency domain. Specifically, coherence elucidates the linear time-invariant relationship between two signals, offering insights into how distinct channels may be interacting or how different brain regions may be synchronized.

The data, obtained from the tEEG setup and organized by channels and time points, underwent a coherence analysis for each possible pair of channels. Given that coherence is computed across various frequencies, an average value was derived for each channel pair to represent their overall synchrony. This resulted in a coherence matrix, which is symmetric by design, capturing the relationships among all channels.

2.4.3 Event-Related Potentials (ERP) Analysis

Event-related potentials (ERPs) are voltage fluctuations resulting from neural activations, closely tied to specific sensory, cognitive, or motor events. They offer a non-invasive method to study the processing of external and internal stimuli in the brain. This section seeks to compare the ERP outcomes from conventional EEG and the emerging tEEG during movement onset. For this specific comparison, ERPs were analyzed in the context of movement onset. We focused on three primary conditions: No Movement, Power Grasp, and Precision Grasp. By aligning the EEG data with the exact moment of movement initiation, we sought to ascertain the brain’s immediate response to these motor activities.

2.4.4 Time-Frequency Analysis Using Wavelets

Building upon the foundational analyses of SNR, ERPs, and functional connectivity, we extend our methodological framework to encompass time-frequency analysis using wavelets. While features derived from the time domain, such as ERPs, provide valuable insights into neural dynamics, they offer a limited perspective on the intricate oscillatory nature of brain signals. To capture a more comprehensive feature map, it is imperative to consider both the time and frequency characteristics of the EEG and tEEG data.

We employed time-frequency analysis using wavelets, which allows for the decomposition of EEG and tEEG signals into time and frequency domains simultaneously. This approach is particularly adept at identifying non-stationary signals, which are common in EEG data associated with motor tasks. For our analysis, we utilized the Morlet wavelet, a commonly used wavelet in neuroscience due to its biological relevance and ability to provide a good balance between time and frequency localization. The continuous wavelet transform (CWT) was applied to the preprocessed signals from both EEG and tEEG data to obtain the time-frequency representation of the underlying neural activity.

In our computational approach, we first determined the power of the wavelet coefficients by taking their absolute values and squaring them. This step was crucial for emphasizing the energy content at each frequency and time point. Subsequently, we averaged these power values across all trials to yield a mean spectral density for each channel. The resulting average power spectra were visualized as heatmaps, which allowed for a direct comparison between the EEG and tEEG data. These visual representations were scaled to facilitate a clear comparison, with the color intensity indicating the power at each time-frequency point.

The average power spectra, visualized as heatmaps, serve not only as a tool for feature extraction but also as a means for a detailed comparison between EEG and tEEG. The heatmaps facilitate a side-by-side evaluation of how EEG and tEEG represent neural dynamics across different frequency bands and time intervals. This comparative analysis is crucial, as it allows us to discern which modality provides a richer and more detailed depiction of brain activity, thereby offering superior features for the classification of motor tasks.

2.5 Feature Extraction and Classification

In our previous investigations, comparisons between EEG and tEEG, specifically in terms of SNR and ERPs, have consistently demonstrated the superiority of tEEG. Building upon these findings, the present study aims to further contrast the capabilities of EEG and tEEG in a real-world classification task, thereby bridging the gap between analytical comparisons and practical applications.

The primary objective during the feature extraction phase was to capture relevant information from the EEG and tEEG data. The time window $[-1, 1]$ s was defined as the time region of interest (tROI), with 0 s corresponding to the movement onset. Wavelets, specifically the complex Morlet wavelet (cmor), were employed to decompose these segments into various frequency bands: delta, theta, alpha, beta, and gamma. For each of the identified frequency bands in every channel, four statistical features were extracted from the magnitude of the wavelet coefficients. These features are: Mean of the magnitude, Variance of the magnitude, Skewness of the magnitude, Kurtosis of the magnitude.

Given that there were 4 channels, each channel containing data from 5 frequency bands, and each band producing 4 features, the total feature count amounted to 80 for every data instance. With the features in hand, the subsequent step was classification. We employed four distinct machine learning algorithms: Support Vector Machine (SVM), Random Forest (RF), Extreme Gradient Boosting (XGBoost), and Linear Discriminant Analysis (LDA). These techniques were used for both multiclass and binary classification scenarios, covering a range of hand-grasping situations. To assess the effectiveness of these models, we implemented a 5-fold cross-validation method. This approach helped us gain a reliable measure of the models' ability to generalize, as it calculated the average performance indicators across all the validation folds.

3 Results

3.1 Comparative Analysis

The comparative analysis of SNRs between the tEEG and conventional EEG technologies revealed a consistent pattern favoring the tEEG method across various channels. As delineated in Figure 3, the grand average SNR values for all subjects were assessed at channels P3, C3, C4, and F5. Notably, the tEEG (green boxes) consistently exhibited higher median SNRs across all channels when compared to the conventional EEG (blue boxes). Specifically, the median SNR for the tEEG ranged from 56.24 dB at channel C3 to 59.56 dB at channel P3, which was the highest observed across all channels and technologies. In comparison, the conventional EEG technology presented lower median SNRs, with the lowest at channel C4 (53.92 dB) and the highest at channel P3 (54.57 dB). In addition to the superior median SNRs, the tEEG also demonstrated lower variability in SNR measurements among subjects, as evidenced by the narrower interquartile ranges in the green boxes. This reduced variance suggests that the tEEG provides more consistent and reliable SNR values, which is a critical aspect of EEG signal quality.

Figure 4 presents the grand average functional connectivity between EEG channels, quantified across all subjects for both EEG and tEEG technologies. The heatmaps visually compare the con-

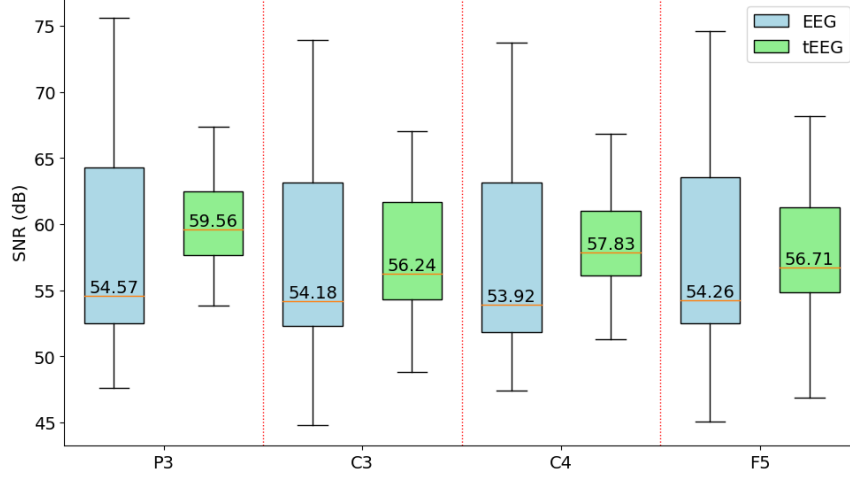


Figure 3: Box plot representation of grand average SNR across P3, C3, C4, and F5 channels, comparing tEEG (green) to EEG (blue).

nectivity strengths, with conventional EEG displayed on the left and tEEG on the right. The conventional EEG heatmap shows considerable functional connectivity, with several channel pairs exhibiting strong correlations, such as P3-F5 (0.82) and C3-F5 (0.8), suggesting significant shared signal components across these channels. This is indicative of a lower spatial resolution, where the activity from different brain regions may be detected simultaneously by multiple channels. Conversely, the tEEG heatmap illustrates substantially lower connectivity values for all channel pairs when compared to conventional EEG. This is particularly evident in the markedly reduced correlations for channel pairs P3-F5 (0.01) and C3-F5 (0.048). The overall lower connectivity values in the tEEG heatmap underscore its higher spatial resolution, demonstrating its ability to more effectively discriminate between the electrical activities of different brain areas.

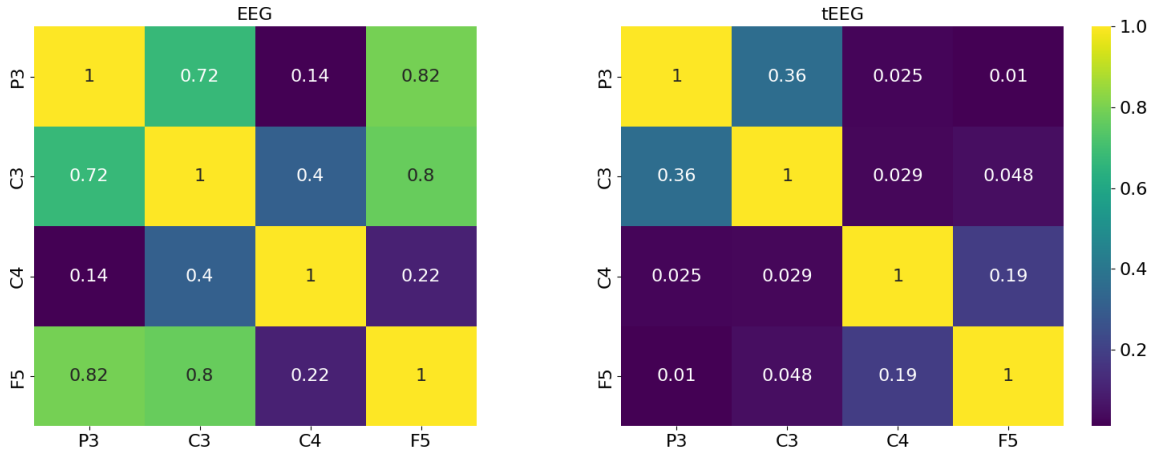


Figure 4: Heatmaps of grand average functional connectivity across EEG channels for EEG (left) and tEEG (right).

Figure 5 contrasts the ERPs and Global Field Power (GFP) between EEG and tEEG for subject 1 as an example. The first row represents data from conventional EEG, while the second row displays results from tEEG. The conditions compared across columns include No Movement, Power Grasp, and Precision Grasp, with time zero marking the onset of movement. During the No Movement condition, both technologies demonstrate baseline neural activity with flat ERP traces and low GFP fluctuations, as anticipated when no motor action is performed. This condition establishes a comparative rest state for subsequent analyses of neural dynamics. The Power Grasp condition reveals a stark contrast between the EEG technologies at the moment of movement onset. Conventional EEG captures a clear peak in the ERP waveform, with a corresponding GFP elevation indicative of neural engagement. However, tEEG exhibits a more sharply defined ERP peak and a crisper GFP response, suggesting its enhanced capability to detect the neural activation associated with the grasping motion. For the Precision Grasp, the distinction between EEG and tEEG is even more pronounced. EEG captures the ERP response adequately, but tEEG delineates more intricate fluctuations in the ERP waveforms across channels, as shown by the varied trace colors. The GFP for tEEG is more complex, particularly around the movement onset, highlighting its potential to resolve finer neural responses related to the intricate motor task of precision grasping.

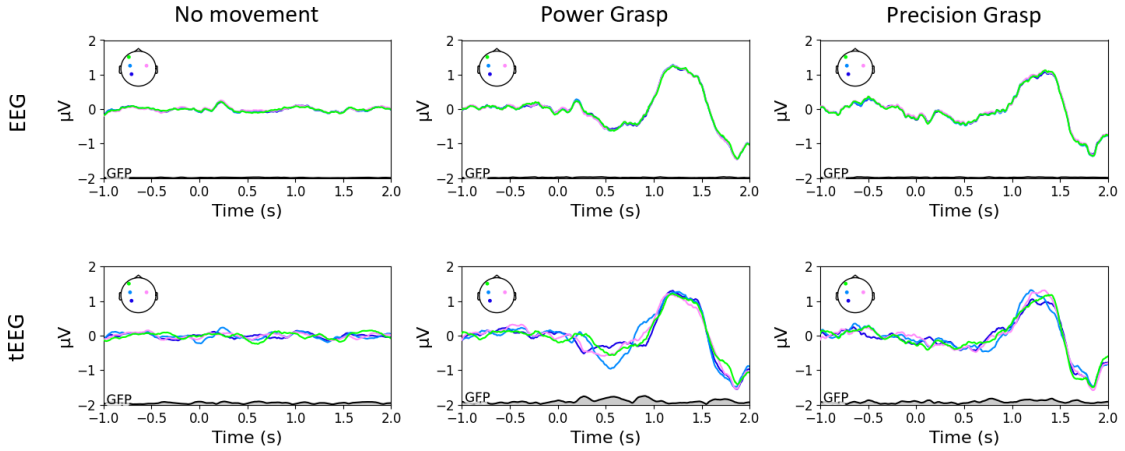


Figure 5: Comparison of ERPs and Global Field Power (GFP) between EEG (top row) and tEEG (bottom row) across three motor tasks.

Figure 6 showcases the wavelet time-frequency representations for conventional EEG and tEEG, analyzing the neural dynamics from one second before to one second after the onset of movement, which is marked by time zero on the x-axis. During the Power Grasp and Precision Grasp conditions, the time-frequency maps exhibit a high increase in activity, particularly noticeable around 500ms post-movement onset. The tEEG maps display a more pronounced increase in activity across a range of frequencies when compared to conventional EEG. This increased activity, especially evident in the beta frequency band, is indicative of the sensorimotor processing associated with the execution of the grasping tasks. In the No Movement condition, conventional EEG exhibits minimal activity, aligning with expectations of neural quiescence. However, tEEG reveals subtle low-frequency activities even

in this resting state, indicating its heightened sensitivity to neural oscillations that conventional EEG may not capture. The observed differences in the time-frequency domain between EEG and tEEG underscore the potential of tEEG to provide enhanced temporal and spectral resolution, which could translate to more accurate identification of distinct neural patterns associated with various motor tasks.

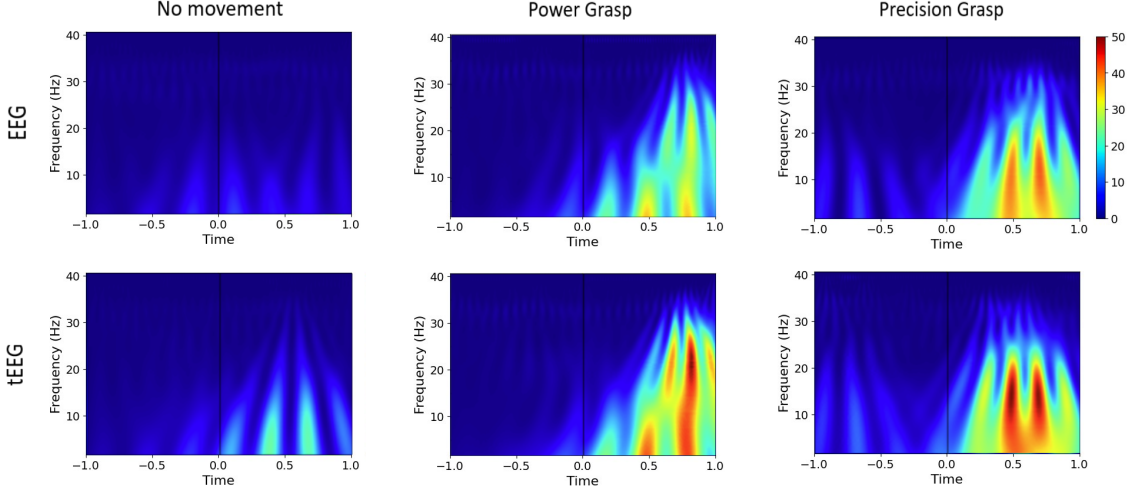


Figure 6: Wavelet time-frequency maps comparing EEG (left column) to tEEG (right column) for Power Grasp (top row), Precision Grasp (middle row), and No Movement (bottom row) conditions.

3.2 Feature Extraction and Classification

Table 1 presents the binary classification accuracies for distinguishing between No-movement and Power Grasp tasks across different subjects using various machine learning models with accuracies reported for both conventional EEG and tEEG. Across all subjects, tEEG consistently outperformed conventional EEG in classification accuracy. The mean accuracy improvements with tEEG ranged from 3.76% in SVM to a notable 16.30% in LDA, indicating a substantial enhancement in the machine learning models’ ability to utilize the data captured by tEEG. The Random Forest classifier achieved the highest mean accuracy for tEEG at 91.53%, which underscores the effectiveness of this model in conjunction with the high-resolution data provided by tEEG. Similarly, LDA showed the least improvement, yet still produced a mean accuracy increase of 16.30% with tEEG. Individual subject analysis revealed that Subject 7 (S7) exhibited the highest classification accuracy with tEEG at 98.33% using the XGBoost model, while the lowest was for Subject 10 (S10) at 67.5% using LDA.

Table 2 details the binary classification accuracies for No-movement versus Precision Grasp tasks, utilizing a range of machine learning models and comparing the performance between conventional EEG and tEEG. The data illustrate a consistent trend where tEEG provides a marked improvement in classification accuracy over conventional EEG. The mean accuracies are notably higher with tEEG, exhibiting an increase of 12.98% for Random Forest, 8.84% for SVM, 15.65% for XGBoost, and 15.21% for LDA. The XGBoost classifier shows the most substantial average increase in accuracy

Table 1: Binary Classification Accuracies for No-movement vs. Power Grasp Tasks Using Various Models, Comparing EEG and tEEG Accuracies Across Different Subjects.

| Subjects | Random For. (%) | | SVM (%) | | XGBoost (%) | | LDA (%) | |
|----------|-----------------|--------------|---------|--------------|-------------|--------------|---------|--------------|
| | EEG | tEEG | EEG | tEEG | EEG | tEEG | EEG | tEEG |
| S1 | 70 | 90 | 75 | 75.56 | 73.33 | 88.89 | 51.67 | 78.89 |
| S2 | 82.82 | 87.42 | 76.54 | 85.42 | 84.36 | 84.32 | 56.28 | 72.89 |
| S3 | 71.76 | 92.36 | 74.05 | 83.3 | 76.34 | 90.17 | 50.26 | 84.1 |
| S4 | 95 | 96.11 | 89.17 | 85.56 | 90.83 | 97.22 | 68.33 | 76.67 |
| S5 | 69.58 | 90.56 | 69.17 | 68.06 | 67.08 | 86.11 | 60.42 | 69.44 |
| S6 | 80 | 91.33 | 73 | 78.67 | 76 | 88.67 | 43 | 78.67 |
| S7 | 94.38 | 98.24 | 93.12 | 96.67 | 92.5 | 98.33 | 84.38 | 89.58 |
| S8 | 73.75 | 89.58 | 70 | 70 | 71.25 | 90 | 66.88 | 73.75 |
| S9 | 73.12 | 91.67 | 67.5 | 72.92 | 65.62 | 90 | 59.38 | 72.08 |
| S10 | 68.12 | 87.08 | 66.88 | 75.83 | 68.12 | 82.5 | 60 | 67.5 |
| Mean | 77.85 | 91.53 | 75.44 | 79.20 | 76.54 | 89.62 | 60.06 | 76.36 |

when using tEEG, highlighting the synergy between this model and the high-resolution data from tEEG. Notably, every subject experienced an accuracy improvement with tEEG, affirming its universal enhancement of classification performance. Subject 7’s results stand out with an exceptional 99.17% accuracy using the Random Forest classifier in conjunction with tEEG, while the lowest accuracy with this technology is seen in Subject 8, with 67.50% using LDA. This spread suggests that while tEEG generally improves classification outcomes, the extent of its impact can vary among individuals.

Table 2: Binary Classification Accuracies for No-movement vs. Precision Grasp Tasks Using Various Models, Comparing EEG and tEEG Accuracies Across Different Subjects.

| Subjects | Random For. (%) | | SVM (%) | | XGBoost (%) | | LDA (%) | |
|----------|-----------------|--------------|---------|--------------|-------------|--------------|---------|--------------|
| | EEG | tEEG | EEG | tEEG | EEG | tEEG | EEG | tEEG |
| S1 | 76.67 | 90 | 78.33 | 85.56 | 78.33 | 90 | 51.67 | 71.11 |
| S2 | 78.08 | 88.53 | 62.56 | 82.21 | 67.18 | 84.37 | 53.21 | 76.11 |
| S3 | 75.03 | 93.22 | 62.35 | 82.56 | 66.99 | 93.19 | 48.95 | 71.2 |
| S4 | 93.33 | 92.78 | 88.33 | 82.22 | 91.67 | 92.22 | 64.17 | 77.78 |
| S5 | 70.42 | 88.89 | 72.08 | 76.94 | 69.17 | 84.72 | 63.33 | 69.72 |
| S6 | 80 | 88.67 | 67 | 87.33 | 75 | 90.67 | 62 | 76 |
| S7 | 93.75 | 99.17 | 92.5 | 94.58 | 93.12 | 97.92 | 80.62 | 92.92 |
| S8 | 68.12 | 89.58 | 70.62 | 73.33 | 64.38 | 88.75 | 54.37 | 67.50 |
| S9 | 70.62 | 89.17 | 68.12 | 77.08 | 67.5 | 88.75 | 65 | 70.42 |
| S10 | 71.25 | 87.08 | 69.38 | 77.92 | 67.5 | 86.67 | 54.37 | 77.08 |
| Mean | 77.73 | 90.71 | 73.13 | 81.97 | 74.08 | 89.73 | 59.77 | 74.98 |

Table 3 summarizes the binary classification accuracies for discriminating between Power Grasp and Precision Grasp tasks, utilizing various machine learning models for both conventional EEG and tEEG. A key observation from the table is that while tEEG demonstrates an overall improvement

in classification accuracy for most models, the SVM model with conventional EEG data exhibits a slightly higher average accuracy (75.53%) compared to tEEG (74.23%). However, this trend does not hold across other models. The XGBoost classifier, in particular, shows a marked increase in mean accuracy from 72.59% with EEG to 86.59% with tEEG. This substantial improvement highlights the potential for tEEG to enhance classification performance when paired with models that can exploit its higher-resolution data. Subject 7’s near-perfect classification with tEEG using Random Forest underscores this potential. For Random Forest and LDA models, tEEG also outperforms conventional EEG, with mean accuracies higher by 13.28% and 12.41%, respectively. These results illustrate the capacity of tEEG to provide more discernible patterns of neural activity, which these algorithms can leverage to differentiate between motor tasks more effectively.

Table 3: Binary Classification Accuracies for Power Grasp vs. Precision Grasp Tasks Using Various Models, Comparing EEG and tEEG Accuracies Across Different Subjects.

| Subjects | Random For. (%) | | SVM (%) | | XGBoost (%) | | LDA (%) | |
|----------|-----------------|--------------|--------------|-------|-------------|--------------|---------|--------------|
| | EEG | tEEG | EEG | tEEG | EEG | tEEG | EEG | tEEG |
| S1 | 65 | 82.22 | 73.33 | 76.67 | 63.33 | 78.89 | 40 | 67.78 |
| S2 | 64.1 | 87.47 | 67.18 | 71.79 | 61.03 | 84.32 | 48.21 | 72.74 |
| S3 | 73.86 | 89.37 | 78.3 | 79.6 | 71.57 | 87.92 | 60.26 | 76.47 |
| S4 | 90.83 | 95.56 | 90 | 80.56 | 87.5 | 94.44 | 64.17 | 66.11 |
| S5 | 72.92 | 86.94 | 72.5 | 65.56 | 71.25 | 85.83 | 62.5 | 66.39 |
| S6 | 78 | 89.33 | 69 | 76 | 75 | 88.67 | 61 | 69.33 |
| S7 | 91.88 | 97.92 | 88.75 | 85.83 | 90 | 97.08 | 80 | 77.08 |
| S8 | 69.38 | 85.83 | 73.12 | 64.17 | 75 | 85.83 | 53.75 | 71.25 |
| S9 | 69.38 | 82.92 | 70.62 | 72.92 | 66.25 | 82.08 | 54.37 | 64.17 |
| S10 | 70.62 | 81.25 | 72.5 | 69.17 | 65 | 80.83 | 47.5 | 64.58 |
| Mean | 74.60 | 87.88 | 75.53 | 74.23 | 72.59 | 86.59 | 57.18 | 69.59 |

Table 4 summarizes the classification accuracies for a multiclass scenario involving No-movement versus different grasp tasks, contrasting the performance between EEG and tEEG across various subjects and machine learning models. It is notable that almost all classification results exceed the chance level of 33.33%, indicating that both EEG and tEEG provide signals containing sufficient information to distinguish between the classes above a level of random guessing. This is an important baseline as it establishes that the neural signals being classified carry task-relevant information. tEEG consistently shows an advantage over conventional EEG across all subjects and models, with the mean accuracy for tEEG being notably higher. The Random Forest classifier in particular reveals a substantial mean accuracy increase from 47.06% with conventional EEG to 72.51% with tEEG. The performance of the SVM model exhibits robustness across both EEG and tEEG modalities, with nearly identical average results, although EEG displays a marginally higher accuracy. XGBoost and LDA models further reinforce this trend, showing substantial improvements when using tEEG data, with mean accuracies of 75.97% and 63.46% respectively.

The bar plot in Figure 7 illustrates the improvement in classification accuracy achieved by using tEEG over conventional EEG for various binary and multiclass tasks. Each bar represents the

Table 4: Multiclass Classification Accuracies Across Different Subjects for No-movement vs. Power Grasp Tasks, Comparing EEG and tEEG Performance for Various Models.

| Subjects | Random For. (%) | | SVM (%) | | XGBoost (%) | | LDA (%) | |
|----------|-----------------|--------------|--------------|-------|-------------|--------------|---------|--------------|
| | EEG | tEEG | EEG | tEEG | EEG | tEEG | EEG | tEEG |
| S1 | 38.67 | 63.7 | 57.33 | 51.85 | 41.33 | 79.26 | 20 | 72.59 |
| S2 | 36.25 | 70.91 | 56.25 | 58.28 | 47.5 | 76.31 | 33.75 | 63.94 |
| S3 | 47.27 | 76.78 | 60.91 | 68.12 | 55.45 | 76.29 | 37.27 | 71.77 |
| S4 | 63.33 | 75.19 | 72 | 67.04 | 68 | 87.04 | 43.33 | 75.56 |
| S5 | 42 | 68.89 | 61 | 57.22 | 46.33 | 65 | 46.33 | 50.56 |
| S6 | 53.6 | 72.44 | 59.2 | 63.11 | 58.4 | 79.11 | 35.2 | 61.33 |
| S7 | 63 | 84.72 | 68.5 | 73.89 | 66.5 | 82.22 | 69 | 70.83 |
| S8 | 42.5 | 71.67 | 60 | 49.17 | 48 | 73.89 | 39.5 | 60.56 |
| S9 | 40 | 70 | 60 | 58.06 | 43.5 | 73.61 | 46 | 53.61 |
| S10 | 44 | 70.83 | 57.5 | 54.44 | 46 | 66.94 | 38 | 53.89 |
| Mean | 47.06 | 72.51 | 61.27 | 60.12 | 52.10 | 75.97 | 40.84 | 63.46 |

percentage increase in accuracy across different machine learning models. The data suggest that while SVM is relatively robust, with smaller improvements seen with tEEG in some scenarios, the other models exhibit substantial accuracy enhancements when employing tEEG. Specifically, the improvement is more pronounced for RF, XGBoost, and LDA models. Furthermore, the bar plot clearly indicates that the superiority of tEEG is more pronounced in complex classification tasks. In the context of multiclass classification, where the task difficulty is inherently higher due to the increase in the number of classes, the advantages of tEEG become more evident. For instance, the RF model shows a remarkable improvement, which is the highest across all tasks and models represented.

4 Discussion

This study corroborates the enhanced proficiency of tEEG over conventional EEG in grasping movement decoding, which is crucial for BCI systems. Aligning with prior research [31, 32], tEEG showed superior spatial resolution and signal-to-noise ratio, with reduced channel crosstalk in functional connectivity and ERP analyses. Further, the ERP data from both conventional EEG and tEEG reveal a distinct neural response to the movement onset across all conditions. However, tEEG seems to offer a more detailed picture, potentially due to its enhanced spatial resolution. The multiplicity of traces in tEEG, especially for dynamic conditions like Power and Precision Grasp, underscores its capability to capture a broader spectrum of neural responses. In the No Movement condition, the disparity between the two methodologies is most evident. While conventional EEG depicts a steady state, tEEG offers a mosaic of neural activities, suggesting that even in a static condition, the brain is far from inactive.

Uniquely, wavelet time-frequency maps indicated that tEEG captured more pronounced brain activity post-movement. This facilitated the improved accuracy of motor task classification across

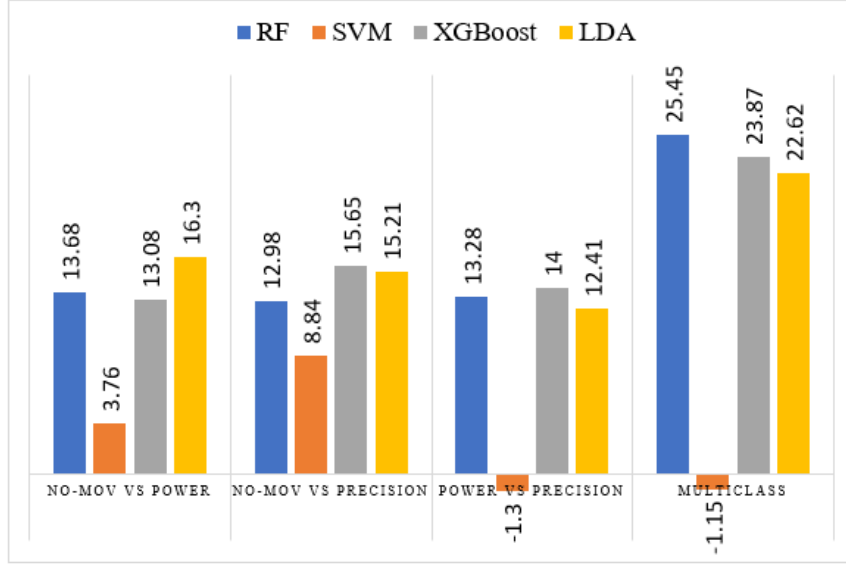


Figure 7: Percentage improvement in classification accuracy using tEEG over conventional EEG for binary and multiclass tasks, across machine learning models.

machine learning models, as demonstrated in the performance enhancements.

The enhanced decoding of grasp movements via tEEG in this study not only aligns with previous research but also surpasses it. tEEG’s benefits in binary classification tasks were particularly significant, with Random Forest and XGBoost showing major accuracy gains. Although SVM performed robustly with both EEG types, tEEG’s enhancements were less pronounced, indicating a need for further study into feature selection for SVM. Importantly, our work achieves up to 91.53% accuracy for No-movement vs. Power Grasp, 90.71% for No-movement vs. Precision Grasp, and 87.88% for multiclass tasks, demonstrating comparable or superior performance to existing research [26–28], even with cost-effective EEG headset. The tEEG’s advantage is most evident in multiclass classification, where it substantially outperforms conventional EEG. Specifically, improvements of 25.45% for RF, 23.87% for XGB, and 22.62% for LDA models highlight tEEG’s capability in handling complex neural pattern distinctions crucial for advanced BCI applications, supporting the necessity for high-fidelity signal capture [50, 51].

5 Conclusion

In conclusion, this study affirms tEEG’s superior capability in decoding grasp movements for BCI applications. Leveraging its higher spatial resolution and signal-to-noise ratio, tEEG outperformed conventional EEG in binary and multiclass classification tasks, supported by notable accuracy gains with machine learning models. The advancements in tEEG technology showcase its potential to enhance BCI functionality, even with cost-efficient setups. Future research should delve into optimizing tEEG for individual neural patterns and exploring its efficacy across various BCI paradigms requiring intricate motor control.

6 Data availability statement

The data collected and analyzed in this study are not openly accessible due to legal and ethical constraints. However, they can be obtained from the corresponding author upon a reasonable request.

7 Acknowledgments

This Research was partially supported by the Rhode Island INBRE program from the National Institute of General Medical Sciences of the National Institutes of Health under grant number P20GM103430 and the National Science Foundation under award ID 2245558. Preliminary results of this study were presented at the Society for Neuroscience 2023 Meeting [52] (November 2023, Washington DC, USA).

8 Conflict of interest

The authors declare that there are no relevant conflicts of interest associated with this paper.

References

1. Wolpaw JR and McFarland DJ. Control of a two-dimensional movement signal by a noninvasive brain-computer interface in humans. *Proceedings of the national academy of sciences* 2004;101:17849–54.
2. Schalk G, McFarland DJ, Hinterberger T, Birbaumer N, and Wolpaw JR. BCI2000: a general-purpose brain-computer interface (BCI) system. *IEEE Transactions on biomedical engineering* 2004;51:1034–43.
3. Abiri R, Borhani S, Sellers EW, Jiang Y, and Zhao X. A comprehensive review of EEG-based brain-computer interface paradigms. *Journal of neural engineering* 2019;16:011001.
4. Castiello U and Begliomini C. The cortical control of visually guided grasping. *The Neuroscientist* 2008;14:157–70.
5. Grafton ST. The cognitive neuroscience of prehension: recent developments. *Experimental brain research* 2010;204:475–91.
6. Gallivan JP, McLean DA, Valyear KF, and Culham JC. Decoding the neural mechanisms of human tool use. *elife* 2013;2:e00425.
7. Castiello U. The neuroscience of grasping. *Nature Reviews Neuroscience* 2005;6:726–36.
8. Park W, Jeong W, Kwon GH, Kim YH, and Kim L. A rehabilitation device to improve the hand grasp function of stroke patients using a patient-driven approach. In: *2013 IEEE 13th International Conference on Rehabilitation Robotics (ICORR)*. IEEE. 2013:1–4.

9. Loureiro RC and Harwin WS. Reach & grasp therapy: design and control of a 9-DOF robotic neuro-rehabilitation system. In: *2007 IEEE 10th International Conference on Rehabilitation Robotics*. IEEE. 2007:757–63.
10. Lamercy O, Dovat L, Yun H, et al. Rehabilitation of grasping and forearm pronation/supination with the Haptic Knob. In: *2009 IEEE International Conference on Rehabilitation Robotics*. IEEE. 2009:22–7.
11. Thrasher TA, Zivanovic V, McIlroy W, and Popovic MR. Rehabilitation of reaching and grasping function in severe hemiplegic patients using functional electrical stimulation therapy. *Neurorehabilitation and neural repair* 2008;22:706–14.
12. Grimm F and Gharabaghi A. Closed-loop neuroprosthesis for reach-to-grasp assistance: combining adaptive multi-channel neuromuscular stimulation with a multi-joint arm exoskeleton. *Frontiers in neuroscience* 2016;10:284.
13. Rupp R, Kleih SC, Leeb R, R. Millan J del, Kübler A, and Müller-Putz GR. Brain–computer interfaces and assistive technology. *Brain-Computer-Interfaces in their ethical, social and cultural contexts* 2014:7–38.
14. Millán JdR, Rupp R, Mueller-Putz G, et al. Combining brain–computer interfaces and assistive technologies: state-of-the-art and challenges. *Frontiers in neuroscience* 2010:161.
15. Lebedev MA and Nicolelis MA. Brain–machine interfaces: past, present and future. *TRENDS in Neurosciences* 2006;29:536–46.
16. Hazrati MK and Erfanian A. An online EEG-based brain–computer interface for controlling hand grasp using an adaptive probabilistic neural network. *Medical engineering & physics* 2010;32:730–9.
17. Chang Y. Architecture design for performing grasp-and-lift tasks in brain–machine-interface-based human-in-the-loop robotic system. *IET Cyber-Physical Systems: Theory & Applications* 2019;4:198–203.
18. Donoghue JP, Sanes JN, Hatsopoulos NG, and Gaál G. Neural discharge and local field potential oscillations in primate motor cortex during voluntary movements. *Journal of neurophysiology* 1998;79:159–73.
19. Schaffelhofer S and Scherberger H. Object vision to hand action in macaque parietal, premotor, and motor cortices. *elife* 2016;5:e15278.
20. Michaels JA and Scherberger H. Population coding of grasp and laterality-related information in the macaque fronto-parietal network. *Scientific reports* 2018;8:1710.
21. Jiang T, Pellizzer G, Asman P, et al. Power modulations of ECoG alpha/beta and gamma bands correlate with time-derivative of force during hand grasp. *Frontiers in neuroscience* 2020;14:100.
22. Fabbri S, Stubbs KM, Cusack R, and Culham JC. Disentangling representations of object and grasp properties in the human brain. *Journal of Neuroscience* 2016;36:7648–62.

23. Perini F, Powell T, Watt SJ, and Downing PE. Neural representations of haptic object size in the human brain revealed by multivoxel fMRI patterns. *Journal of neurophysiology* 2020;124:218–31.
24. Alzubaidi L, Bai J, Al-Sabaawi A, et al. A survey on deep learning tools dealing with data scarcity: definitions, challenges, solutions, tips, and applications. *Journal of Big Data* 2023;10:46.
25. Saeidi M, Karwowski W, Farahani FV, et al. Neural decoding of EEG signals with machine learning: A systematic review. *Brain Sciences* 2021;11:1525.
26. Iturrate I, Chavarriaga R, Pereira M, et al. Human EEG reveals distinct neural correlates of power and precision grasping types. *NeuroImage* 2018;181:635–44.
27. Schwarz A, Ofner P, Pereira J, Sburlea AI, and Müller-Putz GR. Decoding natural reach-and-grasp actions from human EEG. *Journal of neural engineering* 2017;15:016005.
28. Xu B, Zhang D, Wang Y, et al. Decoding different reach-and-grasp movements using noninvasive electroencephalogram. *Frontiers in Neuroscience* 2021;15:684547.
29. Nunez PL, Silberstein RB, Cadusch PJ, Wijesinghe RS, Westdorp AF, and Srinivasan R. A theoretical and experimental study of high resolution EEG based on surface Laplacians and cortical imaging. *Electroencephalography and clinical neurophysiology* 1994;90:40–57.
30. Besio G, Koka K, Aakula R, and Dai W. Tri-polar concentric ring electrode development for Laplacian electroencephalography. *IEEE transactions on biomedical engineering* 2006;53:926–33.
31. Koka K and Besio WG. Improvement of spatial selectivity and decrease of mutual information of tri-polar concentric ring electrodes. *Journal of neuroscience methods* 2007;165:216–22.
32. Aghaei-Lasboo A, Inoyama K, Fogarty AS, et al. Tripolar concentric EEG electrodes reduce noise. *Clinical Neurophysiology* 2020;131:193–8.
33. Toole C, Martinez-Juárez IE, Gaitanis JN, et al. Source localization of high-frequency activity in tripolar electroencephalography of patients with epilepsy. *Epilepsy & Behavior* 2019;101:106519.
34. Makeyev O, Musngi M, Lee F, and Tamayo M. Recent advances in high-frequency oscillations and seizure onset detection using laplacian electroencephalography via tripolar concentric ring electrodes. In: *Proceedings*. Vol. 2. 3. MDPI. 2017.
35. Alzahrani SI and Anderson CW. A comparison of conventional and tri-polar eeg electrodes for decoding real and imaginary finger movements from one hand. *International Journal of Neural Systems* 2021;31:2150036.
36. Vingerhoets G. Contribution of the posterior parietal cortex in reaching, grasping, and using objects and tools. *Frontiers in psychology* 2014;5:151.
37. Makeyev O, Boudria Y, Zhu Z, Lennon T, and Besio WG. Emulating conventional disc electrode with the outer ring of the tripolar concentric ring electrode in phantom and human electroencephalogram data. In: *2013 IEEE Signal Processing in Medicine and Biology Symposium (SPMB)*. IEEE. 2013:1–4.

38. Gramfort A, Luessi M, Larson E, et al. MEG and EEG data analysis with MNE-Python. *Frontiers in neuroscience* 2013;267.
39. Cheveigné A de and Nelken I. Filters: when, why, and how (not) to use them. *Neuron* 2019;102:280–93.
40. Widmann A, Schröger E, and Maess B. Digital filter design for electrophysiological data—a practical approach. *Journal of neuroscience methods* 2015;250:34–46.
41. Widmann A and Schröger E. Filter effects and filter artifacts in the analysis of electrophysiological data. *Frontiers in psychology* 2012;3:233.
42. Carmona RA and Hudgins LH. Wavelet denoising of EEG signals and identification of evoked response potentials. In: *Wavelet Applications in Signal and Image Processing II*. Vol. 2303. SPIE. 1994:91–104.
43. Daubechies I. Ten lectures on wavelets. SIAM, 1992.
44. Mamun M, Al-Kadi M, and Marufuzzaman M. Effectiveness of wavelet denoising on electroencephalogram signals. *Journal of applied research and technology* 2013;11:156–60.
45. Asaduzzaman K, Reaz M, Mohd-Yasin F, Sim K, and Hussain M. A study on discrete wavelet-based noise removal from EEG signals. In: *advances in computational biology*. Springer. 2010:593–9.
46. Cheveigné A de and Arzounian D. Robust detrending, rereferencing, outlier detection, and inpainting for multichannel data. *NeuroImage* 2018;172:903–12.
47. Shoeibi A, Sadeghi D, Moridian P, et al. Automatic diagnosis of schizophrenia in EEG signals using CNN-LSTM models. *Frontiers in neuroinformatics* 2021;15:777977.
48. Hyvärinen A and Oja E. Independent component analysis: algorithms and applications. *Neural networks* 2000;13:411–30.
49. Bell AJ and Sejnowski TJ. An information-maximization approach to blind separation and blind deconvolution. *Neural computation* 1995;7:1129–59.
50. Saha S, Mamun KA, Ahmed K, et al. Progress in brain computer interface: Challenges and opportunities. *Frontiers in Systems Neuroscience* 2021;15:578875.
51. Roman-Gonzalez A. EEG signal processing for BCI applications. *Human–computer systems interaction: backgrounds and applications* 2012;2:571–91.
52. Rabiee A, Ghafoori S, Cetera A, Besio W, and Abiri R. Decoding Reach-to-Grasp Movements: A Comparative study of TCRE and EEG for High-Performance BCI Systems. In: *society for neuroscience*. 2023.